Journal of Advanced Research in Science and Technology
ISSN: 2352-9989

Chemical and Physical Investigations on the barite of Ain Mimoun ore deposit –Khenchela - North-eastern Algeria

K. Abdellaoui [1*], A. Boumaza [1], N. Kamoun [2] , A. Boutaleb [3]

[1] Structures, Properties and Inter Atomic Interactions Laboratory (LASPI²A), Faculty of Science and Technology, University of Abbes Laghrour, Khenchela 40000, Algeria

[2] Université de Tunis El-Manar, Faculté des Sciences de Tunis Département de Physique, Laboratoire de Physique de la Matière Condensée.Tunisia

[3] Laboratoire de Métallogénie et du Magmatisme de l'Algérie, Faculty of Earth Sciences, USTHB, Algiers 16 111, Algeria

Abstract. In this work, we are interested in the barite of Ain Mimoun of the region of the wilaya of Khenchela-Algeria. This ore has not been chemically and physically studied before. This mineral is used in various industries for its special properties: high density, chemical neutrality, whiteness and no abrasive. Among which, it serves as a mineral filler in a wide variety of products including paints, paper, glass, rubber, plastics, friction materials and barriers for protection against radiation. The Ain Mimoun barite deposit remains one of the important sites for the production of barite primarily intended for oil fields as a weighting of the drilling mud. For this purpose, various techniques have been deployed, such as X-ray diffraction (XRD), Fourier Transform Infrared Spectroscopy (FTIR), X-ray photoelectron spectroscopy (XPS), differential thermal (DTA), Thermogravimetric (TG) analysis, and photoluminescence optical properties (PL). Various oxides and / or hydroxides associated with this mineral have been found, especially oxides rich in silice, iron, zinc, copper, etc. The estimation of the quantity of strontium in this barite was proposed in this work. The coexistence of numerous minerals testifies to the richness of this study area.

Keywords: *Barite; XPS analysis; FTIR analysis; TG-ATD analysis; Ain Mimoun ore deposit.*

1. Introduction

Barite exist in various environments ranging from sedimentary to non-sedimentary (hydrothermal and exhalative) conditions [1-2]. Barite is a common mineral in hydrothermal deposits, such it's in the Ain Mimoun ore deposit case. The Ain Mimoun ore deposit is located in the anticline of Djebel Chentgouma, about 25km SW of Khenchela. The vein field occupies the northern flank of a large fold of NE-SW direction. It was discovered in 1968 during a systematic exploration of the region. During the 1972-2005 years, the exploration and extraction in the deposit area have allowed the discovery of new reserves and the entire deposit were estimated at 5.577 million tons barite ore. It is currently mined by an open pit and underground operation. Despite its economic importance very little work has been done on the origin of the Aïn Mimoun ore deposit and characterization of barite from this deposit has never been studied. Nevertheless, we can cite the works cited in references [3], [4], [5], [6], and [7].

* Corresponding author.
E-mail: **maher2009@hotmail.fr** (Abdellaoui K.).
Address: Université Abbes Laghrour, Khenchela 40000, Algérie

Barite is one of the most important industrial minerals. It was noticed due to its high density. Barium Sulfate ($BaSO_4$) is suitable for many diverse applications because of its whiteness, inertness and high specific gravity[8]. Given to its various applications, its large reserves and its intensive use, it contributes significantly to the economic and industrial development of the country. Barium sulfate is a kind of important inorganic chemical product as packing and additive in painting, coating, plastics and medicines fibers [9-10-11]. Barite is one of the most important fillers used in the plastics, rubber and paint industries, and is also used in pharmaceutical formulations [12-13-14]. The field of use of this mineral is versatile, it includes in oil drilling, hydraulic, battery industry and the chemical (paint) and fluoroscopy, protective barrier against radiation, glassware, employed also in dense concrete, it is also used as an inert filler in the friction materials such as brake pads and clutch disc. Among other things, it can be used as a gas sensor for vacuum tubes, lubricant (additive), filler and paper dye. To this end, the mining industry in Algeria is responsible for the operation of this type of ore. Besides the barite veins, one meets several indices as the mineralization of copper, lead, quartz, calcite, etc. Quartz (SiO_2), the dioptase ($CuSiO_3$, H_2O), chalcopyrite ($CuFeS_2$), sphalerite (ZnS), Cinnabar (HgS), calcite ($CaCO_3$), iron hydroxides (Fe_2O_3, H_2O), and the malachite and azurite ($Cu_2CO_3(OH)_2$).This study is based on a set of experimental chemical-physical techniques to characterize this mineral from the region of khenchela and also to know the acolyte products. Thus we present and analyze the results of X-ray diffraction, XPS, FTIR, and DTA-TG analysis.

2. Characterization of samples

All the samples are then characterized using XRD, SEM observations and qualitative analysis, FTIR spectroscopy, XPS spectroscopy, and DTA-TG analysis.

-**X-ray diffraction analysis** is performed with a PANalytical X'Pert ProMRD diffractometer with CuKα radiation (($\lambda(K\alpha1) = 0.15406$ nm, $\lambda(K\alpha2) = 0.15444$ nm)). Data are collected with steps of 0.021° (2θ).

-**Scanning electron microscope** SEM microscope (JEOL 7500-F) was used, equipped by Genesis EDX spectroscopy system that was used to measure the composition of the elements constituting the mineral.

-XPS analysis An XPS K-Alpha spectrometer was used to qualitatively and quantitatively verify the composition of the different powder compounds. The spectra were treated using the Thermo advantage V5.27 software. The photoelectrons are excited using a monochromatic Al Kα radiation as the excitation source, collected at $\theta = 0°$ with respect to the surface normal and detected with a hemispherical analyze. The spot size of the XPS source on the sample is 200 µm, and the analysis is operated with pass energy of 150 eV for the survey spectra and 20 eV for the accumulation spectra of the core levels. The pressure is maintained below $1x10^{-8}$ Torr during data collection, and the binding energies (Eb) of the obtained peaks are referenced to the C1s signal for C–H, which is set to 285.0 eV. XPS measurements are made with uncertainties of about 0.2 eV.

- Fourier transformation Infrared spectroscopy (FTIR) IR spectra are obtained using a Perkin–Elmer spectrometer at the resolution of 8 cm^{-1}. Fourier transform infrared (FTIR)

technique is used in the transmission mode in the 4000 - 400 cm^{-1} range. For each sample, 120 scans are used. After the oxidation, ~100 µg of the oxides are scraped. The oxide is then compressed together with 23 ± 2mg of KBr in a cold 150 MPa isostatic press (CIP) in order to obtain a 200 - 250 µm thick pellet. All infrared spectra are reporting absorbance (A= - log (I/I_0)) as a function of the incident wave numbers.

- DTA and TGA analysis , barite powders were subjected to differential thermal analysis (DTA) and thermogravimetric analysis (TGA) using NETZSCH STA 409 PC/PG instrument, with α-alumina as the reference material at a heating rate of 10°C/min in azote (flow rate 10 ml/min), sample mass was about 34 mg.

3. Experimental results

3.1. Macrographique observations, and EDX analysis

Barite mineral is soft but heavy, slightly tinged with white, gray, yellow or brownish. Barite is a mineral species composed of barium sulfate BaSO4 formula with traces of Sr, Ca and Pb. On hydrothermal origin, barite presents various compositions. Rich in Pb, Sr, C, Ra, or several of these elements associated with them or other, dedicate this mineral to the multiple uses. This mineral usually crystallizes as flattened crystals, sometimes lamellar. Crystals are tabular, prismatic, and as grainy, platy, and coxcomb aggregates. Crystals may be present in aggregates (typically cleavable), and these crystals are lenticular grouped into rosettes. Macro graphic images are shown in Figure 1, and 2.

Fig.1: Photomacrograph of barite samples; massive barite-whitish (a), Platy tabular barite (b), barite crystal rosette (c).

Fig.2: The photomacrograph of the barite samples; inlaid barite,SiO_2 (a, b), and blue spot known as the azurite mineral (c).

In crystals, lamellar masses, fibrous, grainy and compact. This mineral contains SiO_2 crystals embedded in cavities (Figure 2a, and b). Blue spot are split in surfaces (azurite) as shown in figure 2c.

The SEM analysis (figure 3) confirms the presence of the various components of barite, in this case we can draw Table 1, giving the molar percentages and mass percentages of Ba, O, S, Si, Ca, Mo, Al, Zn, Ti, elements.

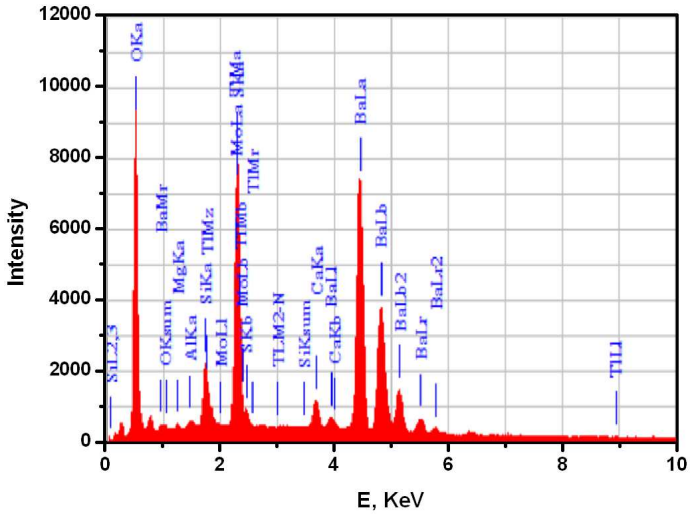

Fig. 3: The EDX spectrum of the raw barite-Ain Mimoun.

Table 1: The EDX analysis of $BaSO_4$ (Ain Mimoun).

Element	KeV	Mass%	Atom%
Al K*	1.486	0.30	0.46
Mg K*	1.253	0.31	0.52
Ti M	2.267	1.44	0.29
Ca K	3.690	1.48	1.49
Si K	1.739	2.24	3.22
Mo L	2.293	4.13	1.74
S K	2.307	10.73	13.50
O K	0.525	24.92	62.81
Ba L	-	Bal	Bal

3.2. X-ray diffraction analysis

Figure.4a. Shows the X-ray diffraction pattern of barium sulphate particles. For the identification of crystal structure and the determination of the particle size, we used X-ray diffraction. All the reflection plains are matched with a orthorhombic phase of barium sulphate [15-16-17], with crystalline cell constants a = 7.144, b = 8.865 and c = 5.445A˚, which are basically in agreement with the reported values (JCPDS Card Files No. 80-0512), space group Pnma.

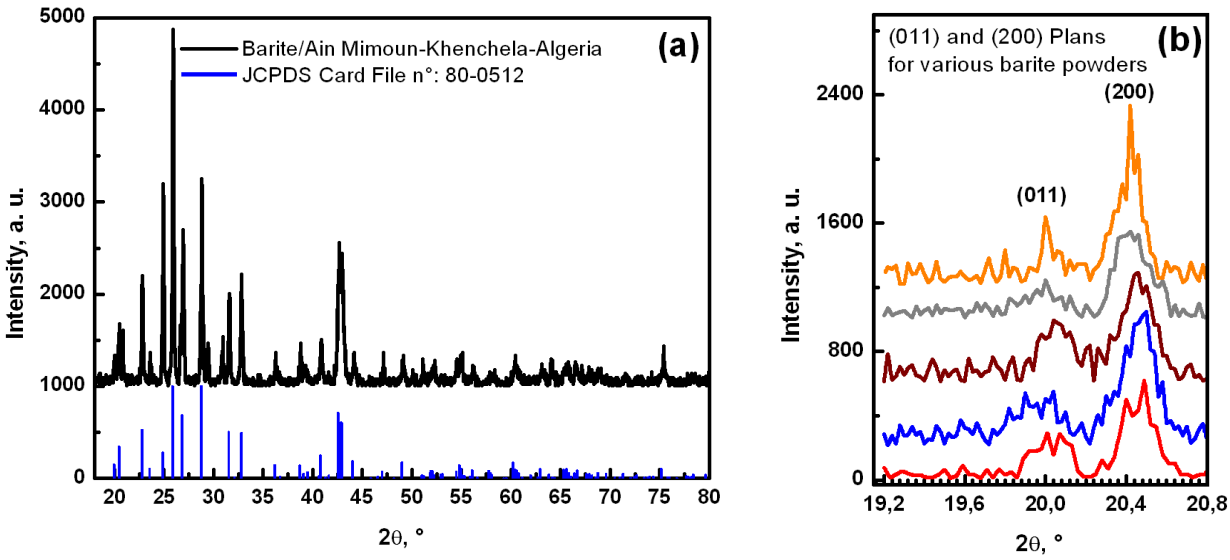

Fig. 4: (a) The X-ray diffraction of barite, (b) X-ray (200) and (011) plans of various barite.

The coexistence of SiO_2 is indicated by the peaks at 2θ = 26.6° and at 20.8°. The small peaks between 29° and 31° may indicate the possible presence of small amounts of complex as battlerite, Azurite, $CaCO_3$, whose elements were analyzed by XPS and EDX, those compounds in oxidized, sulphurised or hydroxide states.

The crystalline sizes of the natural barite are calculated using Scherer's formula [18] for the four high intensity peaks observed at 26.10°, 41.02°, 42.50°, and 44.37 °(2θ) with hkl values (210), (221), (122), and (410). In a first approximation, the full-width at half-maximum β can be expressed as a linear combination of the contributions from the crystallite size, D, and the strain, ε, through the relation

$$\frac{\beta\cos(\theta)}{\lambda} = \frac{1}{D} + \frac{4\varepsilon\sin(\theta)}{\lambda}$$

With λ the X-ray wavelength and θ the Bragg diffraction angle. The values of β and θ parameters are estimated by Gaussian fitting of the XRD peaks. In order to improve the statistics, the (210), (221), (122), and (410) diffractions peaks of barite was used. Results of calculations are given in table 2.

Table 2 : The crystallite size and strain of barite.

Parameter	Crystallite size (nm)	strain
Values	54.53 ± 10.12	0.27±0.05

Qualitative estimation of the amount of $SrSO_4$ by X-ray diffraction:

Qualitative estimation of the amount of $SrSO_4$ in barite was calculed by X-ray diffraction [19]. The molar amount of $SrSO_4$ is possible using this technique. Ratio study of the intensities of the (200) and (011) plans based on strontium content in barite (figure 4b). It was reported by the reference [19] that the intensity of the (011) line decreases with increasing strontium content in barite, finally for 25% higher contents, this peak will confound the (200)

peak. The lines (011) and (200) are shown in figure 4b this reference even gives the relationship.

$$Y = 0, 6. X + 1.7$$

Y being the value of the ratio I(011) / I(200), and X is the mole percentage of $SrSO_4$ in barite. The measure allows the report to determine the content of $SrSO_4$. For a mineral without $CuSO_4$, we have Y= 0, various powders of barite were used, we give the results of the intensities ratios and the percentages of $SrSO_4$ in mol percent in the table below.

Table 3 : The $SrSO_4$ estimation.

	Powder-1	Powder -2	Powder -3	Powder -4	Powder-5
(011) area	8.73	86.28	88.06	55.59	59.57
(200) area	109.31	178.88	173.77	125.09	147.08
$SrSO_4$ mole percent	0.26	0.62	0.45	0.91	1.28
Average value of $SrSO_4$ mole percent			0.79 ± 0.37		

3.3. XPS analysis

Figure 5a shows the XPS survey spectra of the raw barite. For this mineral, the spectrum reveals photoemission peaks for O1s, C1s, S2s, S2p, Ba4d, Ba4p, Ba4s, Ba3d, Ba3p and Ca, which indicates the presence of O, C, S, Ba and Ca on the surface of this compound. The related XPS analysis (Fig. 5a) shows that the binding energies of Ba 3d, S 2p and O 1s are ~778 eV, ~170 and ~531eV, respectively, close to the values of $BaSO_4$ reported in the literature [20-21]. Furthermore, the analysis result also exhibits the atomic percent of Ba, S, O, Ca, and C adventious.

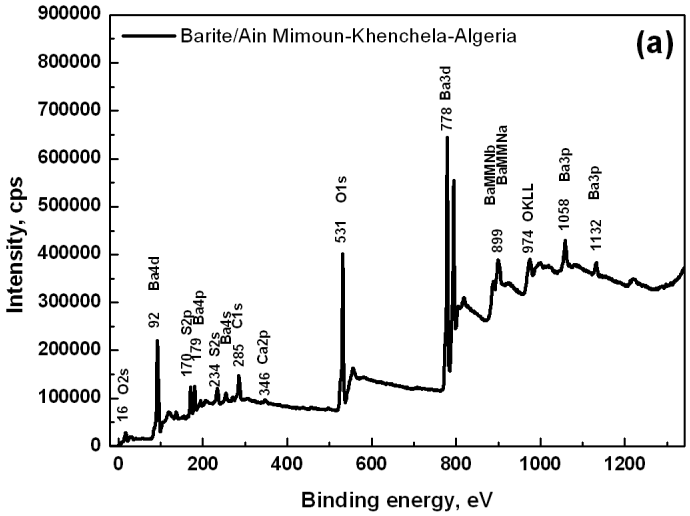

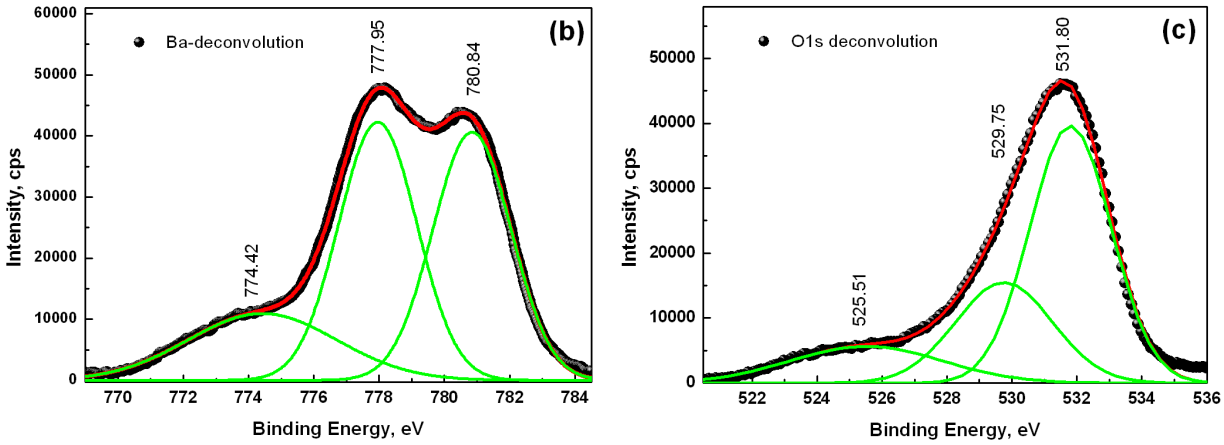

Fig. 5: (a) The XPS spectroscopy of barite (Ain Mimoun-Khenchela), (b and c) XPS spectroscopy of barite core levels of Ba3d and O1s respectively.

The table below gives an estimate of the molar amounts of the elements on the surface of the barite.

Table 4 The Atomic percent of $BaSO_4$ by XPS analysis.

Name	PeakBE (eV)	FWHM (eV)	Area(p) CPS*eV	Atomic %
Ba3d	778	3.78	2358220	12.72
O1s	531	3.85	1612000	44.24
C1s	285	4.01	287318	29.09
Ca2p	346	5.68	56184	1.15
S2p	170	3.19	229896	13.11

It can be seen from figure 4b, that the double peaks for Ba element are at ~780 eV (Ba3d5/2) and ~794 eV (Ba3d3/2), and the binding energies are consistent with the standard values of Ba in $BaSO_4$ [20-21]. The peak around 780 eV can be divided into three peaks at 780.8, 777.9, and 774.4 eV, this type of profile was cited in references [22-23]. The O1s (figure 5c) the energy band can be also divided into three peaks at 531.8, 529.7, and 525.5 eV. These various values of energies reveal the complexity of states (oxides, hydroxides and sulfides) in the raw barite.

Other elements in small amounts can be detected, so we can identify the bands of Si, Zn, Fe, Ti, Na, and also Sr [24-31].

3.4. FTIR Spectroscopy

We analyzed various forms of barites and different parts of this mineral. The spectra obtained can identify not only the barite, but all acolytes compounds. These analyzes were highly effective, in fact we were able to identify all the minerals and oxides present in the environment of the barite.

The spectra show no ambiguity, and reveal the power of this technique. Figure 6a-b shows FTIR spectrum of $BaSO_4$. In this figure many bands can be observed at 3450, 2924, 2850, 2061, 1632, 1384,1180, 1116, 1084, 982, 878, 800, 880, 634, 610, and 474 cm^{-1}. The results are in agreement with those reported in bibliographic data [32-33]. This barite also contains quantities of silicates, azurite, and other minerals revealed in the following figures.

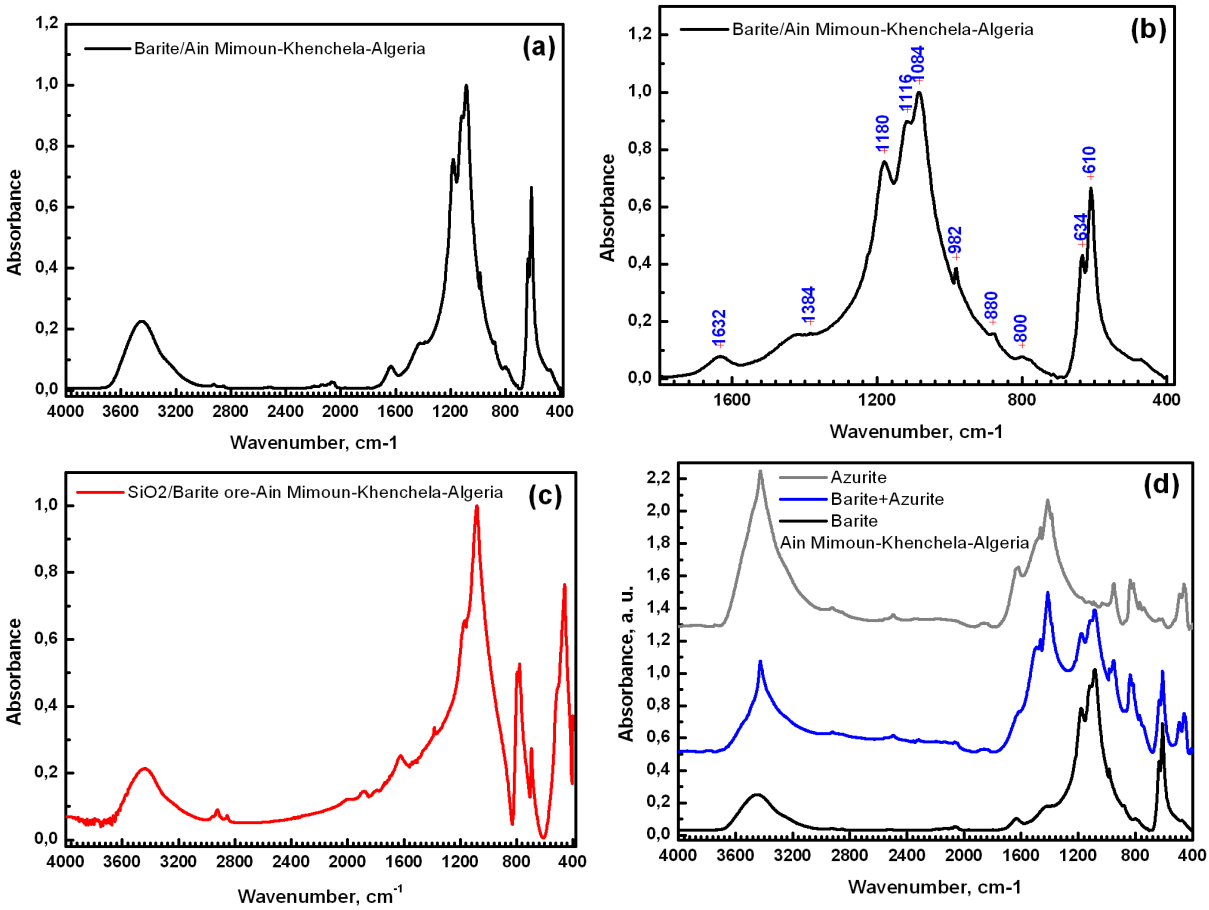

Fig. 6: (a-b) The FTIR spectra of various states of barite (Ain Mimoun), (c) FTIR spectra of SiO_2 embedded in barite, (d) FTIR spectra barite, barite with azurite, and azurite embedded in barite.

The spectrum in figure 6c is relative to the quartz present in the masses of barite. This silicon oxide was removed from the home in barite and then analyzed. In this figure many bands can be observed at 3452, 1622, 1384, 1166, 1082, 796, 778, 694, and 458 cm^{-1} [34-35]. Figure 6d revealed the specter of azurite which is found left as blue spots on the barite (the ore was taken from barite and analyzed). In addition to quartz, azurite, various parts FTIR Specters can confirm the existence of the butlerite ($Fe(SO_4)(OH)\ .2H_2O$), M-OH with hydroxides (M = Fe^{2+} , Mg^{2+} ..), ZnO, and dolomite, Sodium and potassium sulfates ($NaSO_4$-KSO_4) are both measured at 619 cm^{-1}, for Na_2SO_4 and K_2SO_4 the peak correspond to the ν_4 vibration [36-46].

3.5. DTA-TG Analysis

The curves representing the behavior of barite under temperature; TG and DTA are shown in figure 7. Heating was performed from 25°C up to 1400°C. Between room temperature and 200°C, thermogram indicate low weight loss less than 0.16%, which corresponds to the endothermic phenomenon of loss water of hydration (of barium compounds, quartz, and azurites hydrated) and that of any organic matter transformations. Between 200 to 782.7 °C, the TGA thermogram indicate low mass gain of 0.42%, which can be attributed to a low oxidation during this treatment. Between 785.7 and 830°C, the thermal images ATG indicate a mass loss less than 1.4%, which corresponds to the endothermic dehydroxylation phenomenon in compounds contained in barite. At 1169 °C, barite begins its decomposition into BaO. Continuing the slope of the figure corresponding to the TG curve, this decomposition becomes complete between 1550 and 1600 °C. The complete transformation corresponds to a loss of mass equal to 34.30% [47-52].

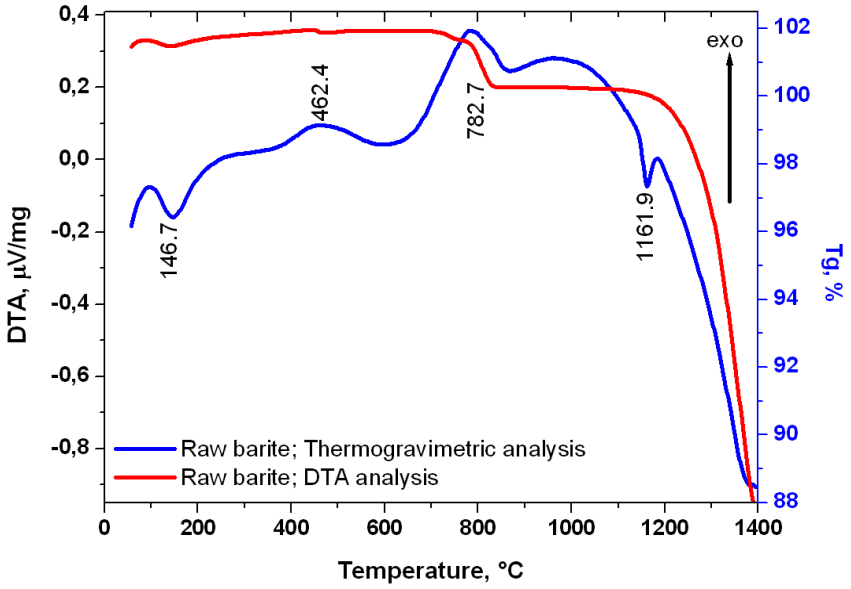

Fig. 7: The DTA and TGA curves of barite (Ain Mimou).

The presence of SiO_2 in significant quantity, small amount of $CaCO_3$, and other compounds as analyzed by FTIR, may lead to some disruption DTA and TG behavior of figures. This around ~ 462.4°C, there is an endothermic phenomenon without loss of mass that reflects the polymorphic transformation of alpha-quartz to α-quartz [53-55].

The presence of dolomite may also cause some processing related to the passage of $MgCa(CO_3)_2$ to give as MgO in the first stage (550-750°C), and CaO in the second stage (870-960°C) [56- 58].

3.6. Photoluminescence spectroscopy

During this study the PL properties of the barite was measured with an excitation wavelength of 266 nm. The figure 8a gives the normalized PL spectra of the mineral.

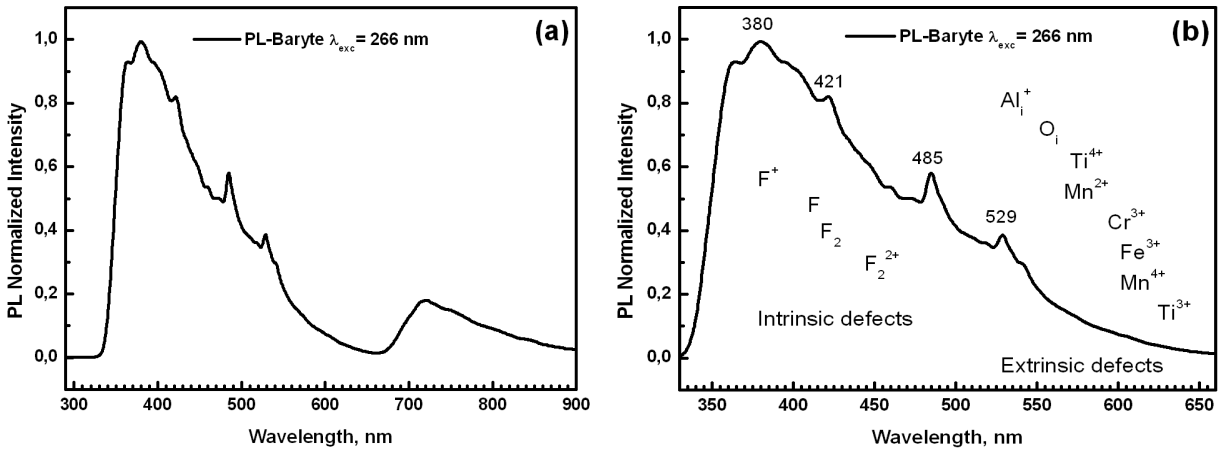

Fig. 8: (a, and b) The PL spectrum at room temperature related to the barite of Ain mimoun, excitation wavelength used λexc = 266 nm.

The characteristic peaks extend into the wavelength region between 370 and 600 nm, signaling that the most intense peaks are between 380 and 550 nm (figure 8b).
Upon 266 nm excitation, a typical PL spectrum consists of several emission peaks:

- Intense violet bands having peaks 380 nm, and 421nm,
- The spectrum also includes blue intense band at 485 nm,
- And the less intense green band at 529 nm.

The origin of these emissions may arise either from intrinsic defects or/and extrinsic defects.

-a- Intrinsic defects

The main intrinsic defect type in oxides (Al_2O_3, ZnO, TiO_2, etc…) is oxygen vacancy; called F centers (Fabre or color center) and it is known that, in the presence of F type defects, UV and visible emission are obtained from the matrix depending on the type of the F centers [59-60-61]. Defects induced in oxides may be of various kinds:
-F centers (oxygen vacancy with two electrons),
-F^+ centers (oxygen vacancy with one electron),
-F_2 centers (two oxygen vacancies with four trapped electrons),
-F^{2+} centers (two oxygen vacancies with three electrons),
-And F_2^{2+}centers (two oxygen vacancies with two electrons) [62].
Also, Al^{i+} centre, which consist of an interstitial aluminium ion having the charge of +1, has been found in α-Al2O3 with emission at 2.4 eV (516.5 nm) in PL spectroscopy [63].

-b- Extrinsic defects

Optical properties of oxide solids are also influenced by metal ions (extrinsic defects), which can appear in quantities below 0.1 wt.%. Ions with an incomplete 3d shell (Ti^{3+}, Cr^{3+}, V^{3+}, Mn^{4+}, Fe^{3+}, Ni^{3+}) substitute for Al^{3+} ions in the α-Al_2O_3 lattice [64-65-66].

According to literature information, we can assign the bands at 380 nm (3.26 eV), 421 nm (2.95 eV), and 485 nm (2.56 eV) to the intrinsic defects corresponding to the oxygen vacancies, and the weaker band at 529 nm (2.34 eV) to possible extrinsic defects.

4. Conclusion

Barite is a common mineral in hydrothermal deposits, which is the case of the Ain Mimoun deposit. It is a mineral that plays a very important role economically, it is found in petrology, chemistry, glass, automotive, paper, medicine, etc. In our work we have characterized this mineral by X-ray diffraction, XPS, FTIR, and also realized thermal analyzes DTA-TG. Physico-chemical analyzes confirmed the coexistence of minerals such as silica, azurite, and dolomite. These encrustations and various oxides, hydroxides, sulfides and carbonates closing elements such as Fe, Zn, Sr, Ti, Ca, Mg, Mo, and Al. The amount of $SrSO_4$ was estimated by X-ray diffraction. Finally, the results of photoluminescence show a predominance of intrisic defects due to oxygen vacancies.

References

[1] M.K. De Brodtkorb. Celestite: worldwide classical ore fields, In: de Brodtkorb, M.K. (Ed.), Nonmetalliferous Stratabound Ore Fields. *Van Nostrand, New York, N.Y* . 1989, 17–39.
[2] R. Abidi, N. Slim-Shimi, C. Marignac, N. Hatira , D. Gasquet , C. Renac , A. Soumarin , S. Gleeson. The origin of sulfate mineralization and the nature of the BaSO4–$SrSO_4$ solid-solution series in the Ain Allega and El Aguiba ore deposits, Northern Tunisia, *Ore Geology Reviews.2012,* 48: 165–179.
[3] R. Laffitte. Etude géologique des Aurès, *Bull, Serv, Carte géol, Algérie*. 1939,15:175-451.
[4] L. Lessard. Faciès béchiques dans le Crétacé supérieur et âge des premières manifestations diapiriques du Trias près de Khenchela, *Publ. Serv. Carte géol. Algérie.1955,* 5: 379-390.
[5] R. Zedam, R. Laouar , S. Bouhlel. Analyse petrographique et sedimentologique de l'albien d'Ain mimoun, Khenchela, Nord-Est Algérie, *Sciences & Technologie D.*2007, 26: 9-20.
[6] O. Haddouche, A. Boutaleb, R. Hebert, D. Picard, L. Sami. Les mineralizations à Pb-Zn, Fe, Ba(Sr) d'El Ouasta (Algérie Nord oriental): Typologie et apport des études d'inclusions fluids, *Bull. Serv. Géol. Algérie*.2004, **15**(2): 87-105.
[7] O. Haddouche, R. Hebert, A. Boutaleb. Géologie, gitologie et microthermométrie des minéralisations à Ba-Pb (ZN,Cu), liées au segment NE du djebel Azreg-djebel Khenchela (Monts des aurès): exemple des gisements d'Ichmoul et d'Ain mimoun, *Bulletin du service géologique national.2010,* **21**(2): 165-182.
[8] H. Bala, W. Fu, Y.Guo, J.Zhao, Y. Jiang and al. In situ preparation and surface modification of barium sulfate nanoparticles, *Colloids Surfaces A:Physicochem. Eng. Aspects.*2006, 274: 71-76.
[9] M. Saraya. Synthesis of $BaSO_4$ Nanoparticles by Precipitation MethodUsing Polycarboxylate as a Modifier, *American Journal of Nanotechnology.2011,* **2**(1): 106-111.
[10] D. Adityawarman, A. Voigt, P. Veit, K.Sundmacher. Precipitation of $BaSO_4$ nanoparticles in a non-ionic microemulsion:Identification of suitable control parameters, *Chem.Eng. Sci.2005,* 60: 3373-3381.
[11] S.C. D'Andrea, , A.Y. Fadeev. Covalent surface modification of calcium hydroxyapatite using n-Alkyl-and n-fluoroalkylphosphonic acids, *Langmuir.2003,* 19: 7904-7910.
[12] H. Bala, W. Fu, J. Zhao, X. Ding, Y. Jiang et al. Preparation of BaSO4 nanoparticles with self-dispersing properties, *Colloids Surfaces A: Physicochem. Eng. Aspects.*2005, 252: 129-134.
[13] A. Kelarakis, and E.P. Giannelis. Crystallization and unusual rheological behavior in poly(ethylene oxide)-clay nanocomposites, *Polymer.*2011, 52: 2221–2227.
[14] B.J. Chisholm, R.B. Moore, G. Barber, F. Khouri, A. Hempstead, M. Larsen, E. Olson, J. Kelley, G. Balch, J. Caraher. Nanocomposites derived from sulfonated poly(butylene terephthalate), *Macromolecules.2002,* 35: 5508–5516.
[15] R.W. James and W.A. Wood. The crystal structure of barytes, Celestine and anglesite, *Proceedings of the Royal society.*1925, **109**(A): 598-620.
[16] V. Ramaswamy, R.M.Vimalathithan, and V.Ponnusamy. Synthesis of monodispersed barium sulphate

nanoparticles using water-benzene mixed solvent, *Adv. Mat, Lett.2012,* **3**(1): 29-33.
[17] W. Gao, B. Zhou, X. Ma, Y. Liu, Z. Wang and Y. Zhu. Preparation and characterization of BaSO4/poly (ethylene terephthalate) nanocomposites, *Colloids and Surfaces A: Physicochem, Eng. Aspects.2011,* 385: 181–187.
[18] B.D. Cullity. Elements of X-ray Diffraction, Addison-Wesley, *Reading, MA*.1972, 350 .
[19] S. Bouhlel. Distribution du baryum et du strontium dans la province fluorée tunisienne; application aux gîtes de Hammam Jédidi et Hammam Zriba-Jebel Guebli ,Thèse de 3ème cycle, *Univers. Toulouse III (inédit)*1982.
[20] Qingde. Chen, Huaying. Bao and Xinghai. Shen. Radiolytic synthesis of BaSO4 microspheres, *Radiation Physics and Chemistry*.2008, 77: 974–977.
[21] J.F. Moulder, W.F. Stickle, P.E. Sobol, K.D. Bomben, In, J Ed and Chastain. Handbook of X-ray Photoelectron Spectroscopy, *Perkin Elmer Physical Electronics Division, Eden*.1992.
[22] V. Craciun and RK. Singh. Characteristics of the surface layer of barium strontium titanate thin films deposited by laser ablation, *Appl. Phys. Lett.2000,* **76**(14).
[23] Ch. Ziegler, G. Frank and W. Gopel . Photoemission study of the Ba core levels in YBa2Cu307_ x. Z, *Phys. B - Condensed Matter.1990,* 81: 349-353.
[24] M. Nerantzaki, M. Filippousi, G. Van Tendeloo, Z. Terzopoulou, D. Bikiaris, OM. Goudouri, R. Detsch, A. Grüenewald and AR. Boccaccini. Novel poly (butylene succinate) nanocomposites containing strontium hydroxyapatite nanorods with enhanced osteoconductivity for tissue engineering applications, *Express Polymer Letters*.2015,**9**(9):773–789.
[25] P. Wang, X. Zhao and B. Li. ZnO-coated CuO nanowire arrays: fabrications, optoelectronic properties, and photovoltaic applications, *Optics Express 11273. OSA.2011,**19***(12).
[26] K. Jradi, C. Maury and C. Daneault. Contribution of TEMPO-Oxidized Cellulose Gel in the Formation of Flower-Like Zinc Oxide Superstructures: Characterization of the TOCgel/ZnO Composite Films, *Appl. Sci*. 2015,5: 1164-1183.
[27] R. Sawyer, H.W. Nesbitt, and R.A. Secco. High resolution X-ray Photoelectron Spectroscopy (XPS) study of K2O–SiO2 glasses: Evidence for three types of O and at least two types of Si, *Journal of Non-Crystalline Solids.2012,* 358: 290–302.
[28] E. Atanassova, and A. Paskaleva. Influence of the rapid thermal annealing in vacuum on the XPS characteristics of thin SiO, *Applied Surface Science.1996,* 103: 359-367.
[29] A.P. Grosvenor, B.A. Kobe, M.C. Biesinger and McIntyre NS. Investigation of multiplet splitting of Fe 2p XPS spectra and bonding in iron compounds, *Surf Interface Anal.2004,* 36:1564–1574.
[30] M. Wegmann, L. Watson, and A. Hendry. XPS Analysis of Submicrometer Barium Titanate Powder, *American Ceramic Society, Journal of the American Ceramic Society, ProQuest Science Journals.2004,* **87**(3): 371-377.
[31] J. C. Dupin, D. Gonbeau, P. Vinatier, and A. Levasseur. Systematic XPS studies of metal oxides, hydroxides and peroxides, *Phys. Chem. Chem. Phys.2000,* 2: 1319-1324.
[32] B. Prameena, G. Anbalagan, V. Sangeetha, S. Gunasekaran, and G.R. Ramkumaar. Behaviour of indian natural baryte mineral, *Int, J. Chem Tech Res.2013,**5***(1): 220-231.
[33] H. Bala, W. Fu, J. Zhao, X. Ding, Y. Jiang, K.Yu, and Z. Wang. Preparation of $BaSO_4$ nanoparticles with self-dispersing properties, *Colloids and Surfaces. A: Physicochem, Eng. Aspects.2005,* 252:129–134.
[34] Y. Shen, Ch. Li, X. Zhu, A. Xie, L. Qiu, and J. Zhu. Study on the preparation and formation mechanism of barium sulphate nanoparticles modified by different organic acids, *J. Chem. Sci, Indian Academy of Sciences*.2007, **119**(4): 319–324.
[35] M. Dimova, G. Panczer, and M. Gaft. Spectroscopic study of barite from the Kremikovtsi deposit (Bulgaria).with implication for its origin, *Annales géologiques de la peninsula Balkanique*.2006,67: 101–108.
[36] J. Manam, and S. Das. Thermally stimulated luminescence studies of undoped, Cu and mn doped $BaSO_4$ compound, *Indian Journal of pure and applied physics*.2009,47: 435-438.
[37] Y. Li, X. Wang, Y. Cui, W. Ma, and H. Guo. High Dispersion Barium Sulfate Nanoparticles Prepared With Dodecyl Benzene Sulfonic Acid, *International Journal of Nanoscience, c World Scientific Publishing Company.2012,* **11**(6): (1240040) 6 pages.
[38] T.M.B. Farias, R.F. Gennari, J.F.D. Chubaci, and S. Watanabe. FTIR spectra and TL properties of quartz annealed at high temperatures, *Physics Procedia*.2009, 2: 493–496.
[39] F. Bosch, Reig, JV. Gimeno Adelantado and MCM. Moya Moreno. FTIR quantitative analysis of calcium carbonate (calcite) and silica (quartz) mixtures using the constant ratio method, *Application to geological samples, Talanta*.2002, 58: 811-821.
[40] L. R. Frost, Martens, N. Wayde, L.L. Rintoul, Mahmutagic, J. Emir, and T. Kloprogge. Raman spectroscopic study of azurite and malachite at 298 and 77 K, *Journal of Raman Spectroscopy*. 2002,**33**(4): 252-259.

[41] S. Vahur, A. Teearu, and I. Leito. ATR-FT-IR spectroscopy in the region of 550–230cm^{-1} for identification of inorganic pigments , *Spectrochimica Acta Part A.2010,* 5:1061–1072.
[42] Cejka, Jiri, Sejkora, Jiri, Plasil, Jakub, Bahfenne, Silmarilly, Palmer, SaraJ, Rintoul, Llewellyn, Frost, L. Ray. A vibrational spectroscopic study of hydrated Fe^{3+} hydroxyl-sulphates; polymorphic minerals butleriteand parabutlerite, *Spectrochimica Acta Part A: Molecular and Biomolecular Spectroscopy* . 2011,**79**(5): 1356-1363.
[43] A.M. Inas, Jawad, A. Ammar, Al-Hamdani, M. Rizgar and A. Hasan. Fourier Transform Infrared (FT-IR) Spectroscopy of Modified Heat Cured Acrylic Resin Denture Base aterial, *International Journal of Enhanced Research in Science, Technology & Engineering ISSN.*2016, **5**(4): 2319-7463.
[44] A. I. Apopei, N. Buzgar and A. Buzat. Raman and infrared spectroscopy of kaersutite and certain common amphiboles, *Analele Stiintifice ale Universitatii "Al. I. Cuza" din Iasi Seria Geologie.2011,* **57**(2): 35–58.
[45] Frost, Ray, Erickson, Kristy, Cejka, Jiri, Reddy and Jagannadha. A Raman spectroscopic study of the uranyl sulphate mineral johannite, *Spectrochimica Acta Part A: Molecular and Biomolecular Spectroscopy.*2005, **61**(11): 2702-2707.
[46] E. D. Chasan, and G. Norwitz. Infrared Determination Of Inorganic Sulfates And Carbonates By The Pellet Technique, *Department Of The Army Zv Frankford Arsenal Philadelphia*, *Pa.*1969: 19137.
[47] B. V. L'vov, L. Valery and Ugolkov. Kinetics of free-surface decomposition of magnesium and barium sulfates analyzed thermogravimetrically by the third-law method, *Thermochimica Acta.*2004, 411: 73–79.
[48] K.H. Stern, and E.L. Weise. High temperature properties and decomposition of inorganic salts, Part 1. Sulfates, *NSRDS-NBS, Washington* . 1966: 7.
[49] S.F. Hulbert. Effect of processing parameters on the kinetics of decomposition of magnesium sulphate, *Mater. Sci. Ing.*1967/1968,2: 262–268.
[50] P. Mohazzabi, and A.W. Searcy. Kinetics and thermodynamics of decomposition of barium sulfates, *J. Chem. Soc., Faraday Trans.1976,*72: 291–295.
[51] BV. L'vov and AV. Novichikhin . Quantitative interpretation of the evaporation coefficients for the decomposition or sublimation of some substances in vacuo, *Thermochim Acta.1997,* 290: 239–251.
[52] B.V. L'vov. The physical approach to the interpretation of the kinetics and mechanisms of thermal decomposition of solids, the state of the art, T*hermochim. Acta*.2001, **373**(2):97–124.
[53] T.A. Aslanian, and A.P. Levanyuk. On the possibility of the incommensurate phase near α-β transition point in quartz, *Solid State Communications*.1979,31: 547-550.
[54] T.A. Aslanian, A.P. Levanyuk, M. Vallade, and J. Lajzerowicz. Various possibilities for formation of incommensurate superstructure near the α-β transition in quartz, *Journal of Physics C—Solid State Physics*.1983,16: 6705-6712.
[55] J.P. Bachheimer. An anomaly in the α phase near the α-β transition of quartz, *Journal de Physique Lettres 4lL.*1980, 559.
[56] B.K. Shahraki, B. Mehrabi, and R. Dabiri. Thermal Behavior Of Zefreh Dolomite Mine, (Centeral Iran), *Journal of Mining and Metallurgy 45B.*2009,(1): 35 – 44.
[57] P. Engler, W. mark Santana, L. martin mittleman and D. Balazs. Non-isothermal in situ xrd analysis of dolomite decomposition, *The Rigaku Journal.1988,* **5**(2).
[58] L. M. Correia, N. S. Campelo, D. S. Novaes, C. L. Cavalcante Jr, J. A. Cecilia, and E. Rodríguez-Castellón. Characterization and application of dolomite as catalytic precursor for canola and sunflower oils for biodiesel production, *Chemical Engineering Journal.2015,* 269: 35–43.
[59] A. Djelloul, A. Boumaza. Peculiarity of the Cathodoluminescence of lpha- Alumina Prepared by Calcination of Gibbsite Powder or Generated by Oxidation of a Metallic FeCrAl Alloy , *INTECH Open Access Publisher -In book: Cathodoluminescence, March*. 2012.
[60] I. Dogan. Fabrication and characterization of aluminium oxide and silicon / aluminium oxide films with Si nanocrystals formed by magnetron co-sputtering technique, Thesis, *school of natural and applied sciences of middle east technical university* .2008.
[61] I. Dogan , I. Yildiz , R.Turana. PL and XPS depth profiling of Si/Al2O3 co-sputtered films and evidence of the formation of silicon nanocrystals, *Physica E.*2009, 41: 976–981.
[62] E.A. Kotomin , A.I. Popov. Radiation-induced point defects in simple oxides, *Nuclear Instruments and Methods in Physics Research B.1998, 141*:1-15.
[63] M. Oja. Dissertationes physicae universitatis tartuensis 110. University of Tartu Press. *https://dspace.ut.ee/bitstream/handle/10062/56291/oja_marek.pdf?sequence=1&isAllowed=y*
[64] V. S. Kortov, V. A. Pustovarov, T. V. Spiridonova, and S. V. Zvonarev. Photoluminescence of ultradisperse alumina ceramics under VUV excitation, *Journal of Applied Spectroscopy.2014,* 80(6): 835-840.
[65] D. O. Ilin, A. S. Vokhmintsev , I. A. Weinstein. Luminescence Characteristics of Nanoporous Anodic Alumina Annealed at Different Temperatures, *Conference Proceedings.2016,*1767-020028.
[66] H. Li. Bubbles propagation in undoped and Titanium (Ti^{3+})-doped sapphire crystals grown by Czochralski (Cz) technique, Cristallography, *Université Claude Bernard - Lyon I.*2014.